Advances in Pharmacological and Pharmaceutical Sciences

WILEY

RESEARCH ARTICLE OPEN ACCESS

The Development of Mung Bean (*Vigna radiata*) Seed Coat Extract Entrapped in Niosome With UVB Protection and Collagen Stimulation

Lattanamixay Souliyanon[1] | Nattawadee Kanpipit[2] | Sakornchon Mattariganont[2] | Suthasinee Thapphasaraphong[2]

[1]Pharmaceutical Chemistry and Natural Products Program, Faculty of Pharmaceutical Sciences, Khon Kaen University, Khon Kaen 40002, Thailand | [2]Department of Pharmaceutical Chemistry, Faculty of Pharmaceutical Sciences, Khon Kaen University, Khon Kaen 40002, Thailand

Correspondence: Suthasinee Thapphasaraphong (sutpit1@kku.ac.th)

Received: 14 September 2025 | **Revised:** 30 January 2026 | **Accepted:** 6 March 2026

Academic Editor: Anjali Chauhan

Keywords: collagen production | mung bean seed coat | niosomes | UVB protection

ABSTRACT

This study aimed to develop a niosome delivery system loaded with mung bean seed coat (MBSC) extract for cosmetic applications. The extract was prepared using Soxhlet extraction with 40% ethanol and demonstrated strong antioxidant activity due to its rich content of phenolic and flavonoid compounds. Twelve different formulations (F1–F12) were prepared using sonication, and their properties, such as entrapment efficiency, particle size, polydispersity index (PDI), and zeta potential, were evaluated. Formulation F12 exhibited the most favorable overall characteristics, demonstrating high entrapment efficiency for phenolics (76.12%) and flavonoids (99.64%), nanoscale particle size (286.43 ± 15.79 nm), acceptable PDI (0.38 ± 0.50), and good physical stability (zeta potential -44.10 ± 1.01 mV). FT-IR analysis confirmed the successful encapsulation of the extract in the niosomal bilayer. Laboratory experiments demonstrated that F12 gradually released the extract and improved skin absorption over 24 h through diffusion. Additionally, HPLC testing confirmed accurate and precise measurements of vitexin and isovitexin, meeting ICH standards for sensitivity and reliability. Furthermore, in vitro studies have demonstrated that the extract effectively protects against UVB-induced cellular damage, thereby supporting its potential application in skincare formulations. These results suggest that Formulation F12 is a safe and effective niosome system with potential for cosmeceutical applications.

1 | Introduction

The use of natural cosmetics has become increasingly important because they offer safer options and are better for the environment compared to chemical-based products. Incorporating natural extracts into skincare products meets the rising demand for products that are both sustainable and health-friendly [1]. MBSC, a by-product of glass noodle manufacturing, has the potential to be reused in the production of skincare products, thereby minimizing waste and lessening environmental pollution. This strategy contributes to environmental conservation by creatively utilizing agricultural leftovers that would otherwise be discarded, turning them into useful materials [2]. This approach not only adds value to agricultural waste but also supports eco-friendly innovations in the cosmetic industry. To further enhance the utility of MBSC, encapsulation in niosome offers several advantages, including improved skin penetration, controlled release of active compounds, and enhanced stability of the extract, making it more effective and suitable for topical application.

Mung bean (*Vigna radiata*), a nutrient-rich legume from the Fabaceae family, is widely cultivated for its nutritional and medicinal value [3]. Despite being widely utilized in traditional

This is an open access article under the terms of the Creative Commons Attribution License, which permits use, distribution and reproduction in any medium, provided the original work is properly cited.

Copyright © 2026 Lattanamixay Souliyanon et al. *Advances in Pharmacological and Pharmaceutical Sciences* published by John Wiley & Sons Ltd.

diets, its seed coat has recently attracted attention due to its remarkable biological qualities, even though it has received little research [4, 5]. Because the seed coat is rich in phenols, flavonoids, alkaloids, and carbohydrates, studies have shown that its ethanolic extracts have better antioxidant, protease-inhibitory, and aldose reductase-inhibitory effects than the cotyledon [5]. Its therapeutic potential is further enhanced by phenolic acids, catechol, and other flavonoids [6, 7].

According to Ref. [7], phenolics and flavonoids, particularly vitexin and isovitexin are the major compounds found in mung bean seed coats (MBSCs). These flavonoids are known for their strong antioxidant effects, which help protect the skin from oxidative stress, a key contributor to aging and damage [8]. Vitexin has been found to neutralize harmful 2,2-diphenyl-1-picrylhydrazyl (DPPH) radicals, protect skin cells from damage caused by UV rays, and inhibit tyrosinase, the enzyme responsible for melanin production [9]. These benefits make vitexin a strong candidate for skincare products that focus on moisturizing, reducing signs of aging, and brightening the skin. Furthermore, ethanol extracts from mung bean seeds have been shown to reduce tyrosinase activity [10].

The combination of bioactive compounds in MBSC extracts makes them strong candidates for use in skincare products, offering powerful antioxidant effects and the ability to enhance collagen production and natural protection of the skin from environmental damage. This discovery creates new opportunities to incorporate this agricultural by-product into cosmeceutical development, merging traditional knowledge with current scientific progress [11].

Nanotechnology enables advanced methods for creating nanoemulsions, liposomes, and niosomes, which improve the permeability, stability, and precise delivery of bioactive compounds. These nanoscale carriers help maintain steady and concentrated levels of active ingredients at the desired location, reducing how often they need to be applied while enhancing their overall effectiveness [12].

Niosomes are nanoscale vesicles made from cholesterol and nonionic surfactants that naturally form in water when the concentration of lipids exceeds the critical micelle concentration. These structures typically use surfactants such as polyglycerol ethers or nonionic alkyl compounds, with cholesterol helping to strengthen and stabilize the bilayer membrane. This arrangement allows niosome to carry both water-soluble and fat-soluble substances. Hydrophilic compounds are retained within the aqueous core of niosome, while lipophilic compounds are embedded within the lipid bilayer. These features make niosomes valuable for drug delivery by protecting active ingredients from degradation caused by oxidation, temperature changes, or pH fluctuations. They also support controlled release and enhance the absorption of ingredients by the skin. Compared to other nanocarrier systems, such as liposomes, niosomes exhibit greater chemical stability because nonionic surfactants are less prone to oxidation than phospholipids. Furthermore, unlike polymeric nanoparticles, which may present cytotoxicity issues, niosomes are generally considered biocompatible and cost-effective to produce at both small and industrial scales [13]. Their ability to extend release times and enhance delivery to the skin makes them especially suitable for topical treatments [14]. Several studies have demonstrated the successful encapsulation of natural plant extracts in niosomes for cosmetic applications. Niosomal formulations of *Zingiber cassumunar*, *Rosmarinus officinalis*, ellagic acid from pomegranate, and anthocyanins have shown enhanced skin penetration, stability, antioxidant activity, collagen stimulation, and photoprotective efficacy compared with nonencapsulated forms [15–17].

However, niosome-based delivery of MBSC extract has not yet been reported in the literature. A by-product of making glass noodles, MBSC is full of healthy phenolic and flavonoid components that have potent antioxidant properties. These characteristics suggest that the extract has significant potential for use in cosmetic formulations, particularly those aimed at protecting and restoring skin. Plant-based polyphenol extracts have been shown in studies to be particularly beneficial in cosmetics and medicinal therapies; their efficacy may be further enhanced by mixing them with advanced delivery technologies such as niosomes. Since several natural plant extracts have already been successfully encapsulated using niosome systems, it stands to reason that the bioactive ingredients of MBSC may be administered with comparable efficiency. Doing so would not only improve their antioxidant and skin-protecting capabilities but also contribute to sustainable product development by giving value to an otherwise discarded material [18].

This research aims to explore the use of niosomes as a delivery system for the MBSC extract, enhancing its application in sustainable skincare and pharmaceutical products. This study highlights the antioxidant, antiaging, and UVB-protective properties of the extract. This strategy not only enhances the extract's functionality and skin delivery, but also satisfies the current skincare industry's growing need for natural, environmentally friendly ingredients. The ultimate objective of this study was to combine cutting-edge nanotechnology with the natural therapeutic potential of MBSC to develop a more potent, long-lasting cosmeceutical.

2 | Materials and Methods

2.1 | Materials

MBSC was obtained from Thai Wah Public Company Limited (Thailand). Acetonitrile (HPLC grade) was obtained from Fisher ChemAlert Guide (USA), while ethanol (analytical grade) and methanol (HPLC grade) were sourced from RCL (Labscan Ltd., Thailand). DPPH, 2,4,6-tris(2-pyridyl)-s-triazine (TPTZ), Folin–Ciocalteu reagent, 2,2′-azino-bis(3-ethylbenzothiazoline-6-sulfonic acid) (ABTS), Trolox, and quercetin were provided by Sigma-Aldrich (USA). Sodium carbonate and ascorbic acid were purchased from Fisher Scientific (USA), and gallic acid was obtained from Merck (Germany). Sodium acetate, ferrous sulfate, and potassium persulfate were supplied by Ajax Finechem (New Zealand), while aluminum chloride and ferric chloride hexahydrate were sourced from Loba Chemie (India). Additionally, 96-well plates were supplied by Thermo Scientific (USA), and syringe filters were obtained from Labfil (China), standard vitexin (purity 99.90%) and isovitexin (purity 99.90%) were purchased from MedChemExpress LLC (USA).

2.1.1 | Equipment

High-performance liquid chromatography (HPLC) was carried out using an Agilent 1260 system equipped with a UV detector (Agilent Technologies, USA) and a 250 × 4.6 mm, 5 μm column

(Phenomenex, USA). Absorbance readings were taken using a microplate reader from PerkinElmer (USA).

2.2 | Methodology

2.2.1 | Preparation MBSC Extract

MBSC was obtained from Thai Wah Public Company in Thailand. The Soxhlet method was used for extraction, with 40% ethanol for 1 h. After the extraction procedure, the solvent was removed using a rotary evaporator, and the residue was freeze-dried. The extract was stored at −20°C until further analysis (Figure S1).

2.2.2 | The Characterization of MBSC Extract

The Folin–Ciocalteu method was adapted to determine the total phenolic content [19]. Gallic acid from a 1 mg/mL stock solution was serially diluted twice in distilled water to create a calibration curve. In a 96-well microplate, 100 μL of a 1:10 diluted Folin–Ciocalteu reagent was mixed with 20 μL of each extract or standard solution (1 mg/mL). 80 μL of a 7% Na_2CO_3 solution was added to the plate after incubation for 6 min. After that, the reaction mixture was left at room temperature in the dark for 30 min. To determine the phenolic content, absorbance was measured at 765 nm.

A colorimetric technique based on quercetin as the standard was used to determine the total flavonoid content (TFC) [19]. By making twofold serial dilutions of quercetin in ethanol, a calibration curve was produced. After adding 20 μL of each extract (1 mg/mL) or standard solution to a 96-well plate, 20 μL of a 10% aluminum chloride solution was added for the assay. Following that, each well received 20 μL of 1 M sodium acetate and 180 μL of distilled water. Absorbance was measured at 415 nm after a 30-min incubation at room temperature. The flavonoid content was determined using the calibration curve.

2.2.3 | The Biological Activities of Antioxidant Assay (DPPH, ferric reducing antioxidant power [FRAP], ABTS)

DPPH radical scavenging method [20]: After preparing a stock solution of L-ascorbic acid (1 mg/mL) in distilled water, it was serially diluted (1–1000 μg/mL). A 96-well plate was filled with 100 μL of each sample and 100 μL of a 0.2 mM DPPH solution, and the plates were left in the dark for half an hour. To determine the percentage of DPPH inhibition, the absorbance was then measured at 517 nm using a microplate reader.

$$\text{Scavenging activity}(\%) = \left[A_{(C)} - \frac{\left[A_{(+S)} - A_{(\text{blank})}\right]}{A_{(C)}}\right] \times 100, \quad (1)$$

where $A_{(C)}$ is the absorbance of the control (distilled water in a DPPH solution). $A_{(+S)}$ is the sample's absorbance with the DPPH solution following the reaction. $A_{(\text{blank})}$ is 40% ethanol absorbance.

The IC_{50} value was determined by plotting the percentage of radical scavenging activity against the corresponding extract concentrations.

Minor adjustments were made to the FRAP assay [21]. Ferrous sulfate (1–1000 μg/mL in methanol) was used to create a standard curve. The FRAP reagent was prepared by combining 300 mM sodium acetate buffer (pH 3.6), 20 mM ferric chloride, and 10 mM TPTZ in a 10:1:1 ratio. A total of 150 μL of FRAP reagent and 50 μL of the sample were added to each well of a 96-well plate. Absorbance was measured at 593 nm after 40 min of dark incubation at room temperature. Antioxidant capacity per gram of extract was measured in mM $FeSO_4$ equivalents/g dry weight (DW).

In accordance with Biskup et al. [21], the ABTS test was used to evaluate the antioxidant activity of the samples. As a positive control, a Trolox stock solution (1 mg/mL) was prepared and diluted to concentrations between 1 and 1000 μg/mL. The ABTS reagent was prepared by combining 6.56 mM ABTS with 2.3 mM potassium persulfate in a 2:1 ratio, then incubating the mixture at room temperature for 16–18 h. Before the assay, the reagent was diluted with deionized water to an absorbance of 0.700 ± 0.020 at 734 nm. The experiment was carried out by adding 50 μL of each sample and 150 μL of the prepared ABTS reagent to a 96-well plate. After a 15-min incubation at room temperature in the dark, the absorbance was measured at 734 nm using a microplate reader. The IC_{50} values were determined by calculating the proportion of radical scavenging activity.

2.3 | The Preparation and Optimization of Niosome With MBSC Extracts

Niosomes were prepared using probe sonication. The surfactant (Span20) and cholesterol (1:1 mM, 2:2 mM, and 3:3 mM) were dissolved in 9 mL of phosphate-buffered saline (PBS pH 5.5) and cosolvents such as propylene glycol (PG) 10% v/v. The MBSC extract was incorporated into the formulation at concentrations of 0% (blank niosomes; F1, F3, F5), 0.25% (F2, F4, F6), 0.5% (F7, F8, F9), and 1% (F10, F11, F12) with controlled heating to promote component melting and ensure homogeneous mixing. The dispersion was homogenized using a probe sonicator (Vibra-Cell, Sonic & Materials Inc., USA) for 10 min at 40°C in a pulsed mode (10-s sonication followed by 10 s pause) at an amplitude of 40%. Entrapment efficiency (%EE), particle size, polydispersity index (PDI), and zeta potential were evaluated for the twelve niosome formulations, as shown in Figure S2 and Table 1.

2.3.1 | %EE of total phenolic content (TPC) and TFC

The EE of phenolic compounds in the niosome was evaluated. The entrapped and nonentrapped phenolic and flavonoid compounds were separated from the niosome by centrifuging it for 30 min using an Amicon 100-kDa cutoff. The entrapped pellet and nonentrapped supernatant were recovered after centrifugation. Using 50% n-propanol, niosome vesicles in the pellet were disrupted to measure the amount of entrapped phenolic and flavonoid contents. The total amounts of phenolics and flavonoids were then determined. The content of phenolic compounds in the pellet was compared to the total phenolic content in the extract to determine the entrapment effectiveness (%) [22].

TABLE 1 | The preparation and optimization of niosome with MBSC extracts.

Formulation	MBSC (%)	Span 20 (mM)	Cholesterol (mM)	PG (%)
F1	—	1	1	10
F2	0.25	1	1	10
F3	—	2	2	10
F4	0.25	2	2	10
F5	—	3	3	10
F6	0.25	3	3	10
F7	0.50	1	1	10
F8	0.50	2	2	10
F9	0.50	3	3	10
F10	1.00	1	1	10
F11	1.00	2	2	10
F12	1.00	3	3	10

Note: F: Formulation of niosome.

$$\text{Entrapment efficiency}(\%\text{EE}) = \frac{\text{amount of encapsulated active compounds}}{\text{total amount in the formulation}} \times 100. \quad (2)$$

2.3.2 | The Size, PDI, and Zeta-Potential Properties

The particle size (nm), zeta potential (mV), and PDI of niosome formulations were measured using a Malvern Zetasizer (Malvern, UK), following established procedures. Zeta-potential values were calculated from electrophoretic mobility using the Smoluchowski equation. These measurements were used to assess the physical properties and stability of the niosome formulations, offering essential information about their potential for further applications [23].

2.3.3 | The Transmission Electron Microscope (TEM)

The morphology of the niosome was used to assess the particle size of the extract-loaded and blank niosome. A 10-μL aliquot of the niosome will be placed on a 200-mesh copper grid for TEM analysis and left to air-dry overnight at room temperature. The dried grid will then undergo TEM imaging in order to accurately determine the size of the particles and analyze the niosome morphology [24].

2.4 | Thermal Stability Study

The thermal stability of niosome formulations was evaluated using a heating–cooling cycle test. Samples stored in glass containers were alternately held at 4°C and 45°C, with each temperature maintained for 24 h over seven complete cycles [22]. Physical stability was assessed by comparing particle size, PDI, zeta potential, and EE (%EE) before and after the test, in accordance with ISO/TR 18811:2018.

2.5 | The Release and Permeation of the Niosome Formulation

The release of phenolic compounds from the niosome formulation was evaluated using a Franz diffusion cell with a Spectra/Por 2/4 dialysis membrane (12,000–14,000 Da). Permeation of phenolic compounds from the niosome formulation was performed using a Franz diffusion cell with a Stat-M membrane. Both experiments were conducted at 37°C with continuous stirring at 800 rpm. The receptor chamber contained 5 mL of 2% Tween 80 solution at pH 5.5, and 1 mL of the niosome formulation was placed in the donor chamber. To maintain sink conditions, 500 μL samples were removed and replaced with an equivalent volume of new receptor medium at 0.5, 1, 2, 4, 6, 8, 12, and 24 h, as specified. Following the analysis of the samples, the percentages of active component released or penetrated were calculated [25].

2.6 | Fourier Transform Infrared (FT-IR) Spectroscopy

Air-dried niosome samples were analyzed by ATR-FT-IR with a Bruker Tensor II spectrometer (Germany). Spectra were obtained in the 4000–650 cm^{-1} range with a resolution of 4 cm^{-1} over 64 scans, as previously reported [25] for the confirmation of encapsulation of niosomes and MBSC extracts.

2.7 | HPLC

HPLC (Agilent 1260) fitted with a C18 stationary phase column (Luna 5μ PFP(2) 100 Å, 250 × 4.6 mm) was used to measure the amount of vitexin and isovitexin in MBSC extract. Using a gradient of Solvents A (1% acetic acid in water) and B (1% acetic acid in acetonitrile) at a flow rate of 1.5 mL/min, the mobile phase was composed of the following steps: 95% A/5% B for 0–20 min, 80% A/20% B for 20–30 min, 78% A/22% B for 30–35 min, 76% A/24% B for 35–40 min, and 95% A/5% B at 40 min [26]. Using a 10 μL injection volume and keeping the column at 30°C, detection was performed by UV–vis at 260–360 nm (Table 2) [27]. Identification was performed by comparing retention times with those of external standards. Calibration curves were constructed using a 1 mg/mL stock solution of vitexin and isovitexin prepared in methanol:water (70:30, v/v). Prior to analysis, all samples and standards were filtered through a 0.45-μm syringe filter. Concentration was

TABLE 2 | Initial findings on the chromatographic separation of vitexin and isovitexin using a C18-Stationary phase (Luna 5u PFP (2) 100A, 250 × 4.60 mm).

Parameter	Condition ($n = 3$)
Mobile phase	Solvent A (1% v/v acetic acid in water) and Solvent B (1% v/v acetic acid in acetonitrile)
Column	Luna 5u PFP(2) 100A (250 × 4.60 mm)
Wavelength	336 nm
Injection volume	10 μL
Detector	Diode-array detector
Run time	40 min
Retention time	Approx.(Vitexin) 21.4 min–(Isovitexin) 22.3 min

calculated using a calibration curve and expressed as milligrams per gram of extract. The HPLC was validated in accordance with ICH guidelines by assessing linearity, accuracy, precision, limit of detection (LOD), and limit of quantification (LOQ). The standard deviation (SD) and slope from the calibration curve were used to calculate LOD and LOQ using formulas $3.3\sigma/S$ and $10\sigma/S$, respectively. Precision was assessed at low, medium, and high concentrations over five consecutive days and within a single day (five duplicates). Accuracy was determined by calculating the percentage recovery at the same concentration levels. MBSC was dissolved in 40% ethanol at 1 mg/mL to prepare the extract, which was then filtered prior to injection. The content of vitexin and isovitexin in the extract was reliably quantified using this method.

2.8 | Cell Line and Culture Conditions

The niosome formulations were evaluated using two human cell lines: human keratinocyte cell (HaCaT) and human foreskin fibroblast (HFF-1). These evaluations assessed cytotoxicity, UVB protection, and collagen production stimulation [28]. An overview of the experimental procedures is provided below.

2.8.1 | Cytotoxicity Testing

HaCaT and HFF-1 cells were grown in Dulbecco's modified eagle medium (DMEM), supplemented with 10% fetal bovine serum (FBS) and 1% antibiotics–antimycotic, at 37°C with 5% CO_2 until they achieved approximately 80% confluence. The cells were allowed to adhere for 24 h after seeding at a density of 1.0×10^4 cells per well into 96-well plates. After that, the cells were treated with niosome formulations and extracts diluted in the culture medium. After 24 h of incubation, cell viability was assessed using the MTT method with a 5 mg/mL MTT solution.

2.8.2 | UVB Protection on HaCaT Cells

HaCaT cells were cultured and seeded into 96-well plates at a density of 1.0×10^4 cells per well. After treatment with niosome formulations and extracts, the cells were exposed to UVB irradiation at a dose of 10 mJ/cm^2 using a UVB lamp, followed by a 24-h incubation. Subsequently, cell viability was assessed *via* the MTT assay to evaluate the protective effects of the formulations against UVB-induced cellular damage [28].

2.8.3 | Collagen Production Stimulation From HFF-1 Cells by Sirius Red Method

HFF-1 cells were cultured and seeded into 96-well plates at a density of 1.0×10^4 cells per well. The cells were then treated with various concentrations of niosome formulations prepared in DMEM supplemented with 10% FBS. The culture medium was sonicated and centrifuged to obtain the collagen-containing pellet following the addition of acetic acid and Sirius Red dye. After the pellet was dissolved in sodium hydroxide, the collagen content was determined by measuring the absorbance at 570 nm [28].

2.9 | Statistical Analysis

Statistical analysis was performed using SPSS software (KKU version). Data are presented as mean ± SD based on three independent replicates ($n = 3$). Differences observed in the stability studies were evaluated using paired sample t tests, and statistically significant differences among experimental groups were determined using one-way analysis of variance (ANOVA). A p value < 0.05 was considered statistically significant.

3 | Results

3.1 | Extraction Results of Mung Bean Seed–Coated Extract

The extraction yield of MBSC was 9.47%, which is considered modest to low. TPC was determined using the Folin–Ciocalteu method, resulting in a value of 15.11 ± 0.34 mg gallic acid equivalents (GAEs) per gram of DW, in line with data that have been previously published [19]. When the aluminum chloride colorimetric assay was used to quantify the TFC, MBSC had the highest TFC, measuring 3.83 ± 0.17 mg quercetin equivalents (QEs)/g DW [19]. Antioxidant activity was evaluated using several assays. The DPPH assay, which assesses radical scavenging capacity [20], showed an IC_{50} value of 36.81 ± 2.48 μg/mL, indicating strong antioxidant potential. Similar results were obtained using the ABTS test [21], yielding an IC_{50} value of 30.59 ± 0.84 μg/mL. Furthermore, the FRAP assay [21], which gauges the extract's capacity to reduce, showed a high reducing power of 17.81 ± 0.74 mM Fe^{2+}/g DW. Table 3 summarizes these results, which bolster the MBSC extract's strong antioxidant qualities.

TABLE 3 | The characterization and antioxidant activities of mung bean seed coated extract (MBSC).

Assay unit	Yield (%)	TPC (mg GAE/g DW)	TFC (mg QE/g DW)	Antioxidant activities		
				DPPH (IC_{50} μg/mL)	ABTS (IC_{50} μg/mL)	FRAP (mM $Fe2^{++}$/g D.W)
MBSC	9.47	15.11 ± 0.34	3.83 ± 0.17	36.81 ± 2.48	30.59 ± 0.84	17.81 ± 0.74

Abbreviation: DW, dry weight.

The 40% ethanol solution was chosen for its appropriate polarity and demonstrated capacity to extract flavonoid and phenolic components, particularly in legumes, where it demonstrated a strong antioxidant recovery [29]. Soxhlet extraction is renowned for its reliable effectiveness in releasing bioactive chemicals by continuous hot solvent cycling, despite its time-consuming and solvent-intensive nature [30].

3.2 | The Evaluation of Niosome

3.2.1 | EE (%), Particle Size (nm), Polydispersity (PDI), and Zeta Potential (mV)

The physicochemical characteristics of niosome formulations prepared by the sonication method are presented in Table 4. All twelve formulations exhibited EEs ranging from 42.97% to 76.24% for TPC, and from 69.33% to 99.64% for TFC. TEM analysis confirmed the formation of spherical niosomal vesicles for both blank and MBSC-loaded formulations (Figure 1). Particle size analysis showed that the formulations ranged from 174.83 nm to 484.00 nm. The PDI ranged from 0.08 to 1.00, indicating a broad size distribution among the formulations, with some displaying high uniformity. Zeta-potential measurements ranged from −29.63 mV to −44.10 mV, suggesting good electrostatic stability of the niosome systems.

Based on the data in Table 4, Formulation F12 was identified as the most suitable due to its high EE (%EE) for both TPC and TFC, recorded at 76.12 ± 0.32% and 99.64 ± 0.60%, respectively, among the highest values observed across all formulations. Its particle size of 286.43 ± 15.78 nm is appropriate for transdermal delivery, while the PDI of 0.38 ± 0.50 indicates acceptable uniformity. The size distribution graph of F12 is presented in Figure S5. The PDI of 0.38 ± 0.50 indicates a polydisperse but acceptable distribution for lipidic nanocarriers intended for topical application [31]. Furthermore, the zeta potential of −44.10 ± 1.01 mV suggests good electrostatic stability. Although Span 20 is nonionic, the niosomes exhibited a negative zeta potential. This is consistent with previous findings where blank nonionic niosomes displayed negative surface charges due to the adsorption of counterions from the aqueous medium [32]. Although formulations F10 and F11 showed comparable %EE and TFC, F10 had an excessively large particle size (484.00 ± 31.12 nm) and a high PDI (1.00), making it unsuitable. While F11 was the size, PDI and zeta potential were less favorable than F12. The selection criteria for the optimal formulation included high EE, particle size below 300 nm, PDI lower than 0.4, and zeta potential greater than ±30 mV. Therefore, F12 was chosen as the most promising formulation for further investigation.

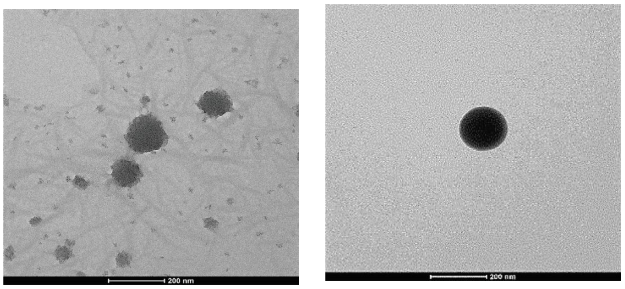
3.2.2 | TEM

The morphology of the niosome formulations prepared by sonication was examined by TEM, with a scale bar of 200 nm (Figure 1). The blank niosome (F5) in Figure 1(a) is depicted as spherical vesicular structures with a nanoscale dimension. MBSC-loaded niosome Formulation F12 in Figure 1(b) is also predominantly spherical, with a smooth surface morphology. Notably, the extract-loaded niosomes appeared slightly larger than the blank niosomes, which can be attributed to the incorporation of the extract within the vesicular bilayer, confirming successful extract loading. The characteristics of both niosomes (F5 and F12) are a homogeneous spherical shape,

TABLE 4 | Entrapment efficiency (%) of total phenolic content, total flavonoid content, size, PDI, and zeta-potential properties.

Formulation	% EE		Size (nm)	PDI	Zeta potential (mV)
	TPC	TFC			
F1	-[a]	-[a]	246.70 ± 14.39[c,d]	0.14 ± 0.09[a]	−32.20 ± 0.36[e]
F2	42.97 ± 8.89[b]	69.33 ± 2.73[b]	230.90 ± 12.55[c]	1.00 ± 0.00[c]	−39.67 ± 1.17[b,c]
F3	-[a]	-[a]	174.83 ± 39.96[a,b]	0.43 ± 0.18[a,b]	−41.00 ± 1.57[b]
F4	61.02 ± 0.81[c]	89.07 ± 9.85[c,d]	215.63 ± 43.78[b,c]	0.45 ± 0.50[a,b]	−34.70 ± 1.74[d]
F5	-[a]	-[a]	162.96 ± 12.65[a]	0.36 ± 0.04[a,b]	−29.63 ± 2.05[f]
F6	67.23 ± 1.02[d]	81.99 ± 12.42[c]	238.70 ± 27.55[c]	0.08 ± 0.06[a]	−31.47 ± 0.76[e,f]
F7	67.50 ± 1.46[d]	93.86 ± 1.54[d,e]	303.66 ± 25.55[e]	1.00 ± 0.00[c]	−41.63 ± 0.91[b]
F8	69.69 ± 0.53[d]	98.14 ± 2.00[e]	229.06 ± 4.89[c]	0.67 ± 0.49[b,c]	−38.47 ± 0.80[c]
F9	68.96 ± 0.34[d]	83.19 ± 1.54[c]	233.00 ± 4.17[c]	0.39 ± 0.27[a,b]	−45.50 ± 0.78[a]
F10	76.24 ± 0.37[e]	98.06 ± 0.77[e]	484.00 ± 31.12[f]	1.00 ± 0.00[c]	−38.00 ± 0.82[c]
F11	69.84 ± 0.85[d]	98.09 ± 2.34[e]	305.36 ± 26.79[e]	0.23 ± 0.11[a,b]	−39.97 ± 0.50[b,c]
F12	76.12 ± 0.32[e]	99.64 ± 0.60[e]	286.43 ± 15.78[d,e]	0.38 ± 0.50[a,b]	−44.10 ± 1.01[a]

Note: Three replicates of zeta potential, particle size, polydispersity index (PDI), and mean entrapment efficiency (%EE) are reported. The same column letters ([a–f]) were used to indicate statistically significant differences using one-way ANOVA at $p < 0.05$.



(a) (b)

FIGURE 1 | The morphology of niosome formulations prepared by sonication was examined using transmission electron microscopy (TEM). The images include (a) blank niosome (F5), (b) MBSC-loaded niosome (F12). The scale bar is 200 nm.

consistent with the typical niosomal structures documented in the literature. For instance, niosomes are spherical, bilayer vesicles that, depending on the formulation and fabrication technique, have diameters ranging from 100 to 300 nm [24, 33].

3.3 | FT-IR Spectroscopy

The FT-IR spectra are presented in Figure S3, and the major characteristic peaks and their assignments are summarized in Table S1. The FT-IR spectrum of the MBSC extract showed several characteristic peaks corresponding to its functional groups (FigureS3A and Table S1). The peak of O–H stretching was observed at 3247 cm^{-1}, while C–H stretching appeared at 2923 and 2855 cm^{-1}. The C=O stretching was detected at 1604 cm^{-1}. In addition, C=C stretching vibrations were observed at 1578 and 1511 cm^{-1}. Bands associated with CH_2 bending were detected at 1393 and 1357 cm^{-1}, along with multiple C–O bands at 1283, 1243, 1183, and 1041 cm^{-1}. Furthermore, various C–H bending vibrations were observed in the range of 993.6 and 413.3 cm^{-1}.

The FT-IR spectrum of the blank niosome (F5) in Figure S3B and Table S1 showed strong vibrational bands including a broad O–H stretching band at 3319 cm^{-1} and C–H stretching peaks at 2971, 2930, 2874, 2382, and 2347 cm^{-1}. A weak C=O stretching band appeared at 1655 cm^{-1}, shifted from the strong ester carbonyl band of single Span 20 at 1738 cm^{-1} (Figure S4A). The C–C stretching appeared at 1463 and 1417 cm^{-1}. The CH_2 bending was observed at 1377 and 1333 cm^{-1}, while various C–O stretching bands were observed at 1284, 1229, 1135, 1076, and 1039 cm^{-1}. The C–H bending vibrations also appeared between 989.4 and 440.5 cm^{-1}, indicating the complex molecular interactions of the blank niosome structure. In comparison, MBSC-loaded niosome (F12) was also confirmed by the presence of distinct vibrational bands in the FT-IR spectrum (Figure S3C and Table S1). A broad O–H stretching band of F12 was observed at 3319 cm^{-1}, similar to F5, and C–H stretching maxima at 2972, 2930, and 2877 cm^{-1} indicated the existence of common functional groups. The C=C stretching (aromatic) appeared at 1610 cm^{-1}, and C–C stretching bands were observed at 1460 and 1413 cm^{-1}. CH_2 bending was noted at 1377 and 1331 cm^{-1}. C–O stretching bands were observed at 1285, 1229, 1135, 1078, and 1039 cm^{-1}, and C–H bending bands appeared from 989.4 to 474.7 cm^{-1}, indicating successful encapsulation and molecular interaction between the extract and the niosome materials.

The FT-IR spectra of each component of the blank niosome, including Span 20, cholesterol, and PG, are shown in Figure S4 and summarized in Table S2. The FT-IR spectrum of Span 20 showed its characteristic IR spectrum (Figure S4A and Table S2), with a broad band of O–H stretching appearing at 3392 cm^{-1} and C–H stretching bands appearing at 2922, 2853, and 2349 cm^{-1}. A strong absorption band was observed at 1738 cm^{-1} corresponding to C=O stretching, while a band at 1560 cm^{-1} was attributed to C=C stretching. Bands associated with C–C stretching were detected at 1462 and 1416 cm^{-1}, and CH_2 bending appeared at 1376 cm^{-1}. C–O stretching bands were observed at 1237, 1168, and 1060 cm^{-1}, while C–H bending peaks appeared between 980.8 and 462.3 cm^{-1}, confirming the presence of aliphatic chains, as expected from the molecular structure of Span 20. The FT-IR spectrum of cholesterol (Figure S4B and Table S2) presented a broad O–H stretching band at 3427 cm^{-1}, along with C–H stretching vibrations, was observed at 2930, 2901, 2867, and 2845 cm^{-1}. The small stretching band for C=O was observed at 1671 cm^{-1}, and C–C stretching was observed at 1463 and 1436 cm^{-1}. Bending of the CH_2 group was observed at 1377, 1365, and 1331 cm^{-1}, and multiple bands for the stretching of C–O were observed between 1274 and 1022 cm^{-1}. Bending vibrations of the C–H bond also occurred between 986.5 and 454.8 cm^{-1}, confirming the aliphatic and steroidal nature of cholesterol. For the FT-IR spectrum of PG (Figure S4C and Table S2), a broad O–H stretching band appeared at 3332 cm^{-1}, reflecting its diol nature. The bands at 2972 and 2877 cm^{-1} were attributed to aliphatic C–H stretching. The absence of a carbonyl peak confirmed the nonester structure, while strong bands observed at 1136, 1076, and 1038 cm^{-1} were assigned to C–O stretching vibrations of alcohol groups.

The FT-IR spectra of the blank niosomes (F5) and MBSC extract–loaded niosomes (F12) are shown in Figure 2. The broad band of O–H stretching appeared at 3319 cm^{-1} in both blank niosome (F5) and MBSC-loaded niosomes (F12), indicating enhanced hydrogen bonding between the phenolic hydroxyl groups of the extract and the hydroxyl groups of the niosomal constituents. Aliphatic C–H stretching bands were observed at 2922, 2930, and 2877 cm^{-1} in MBSC-loaded niosomes, similar to those of the blank niosomes (2971, 2930, and 2874 cm^{-1}). The blank niosome exhibited a characteristic absorption band at approximately 1655 cm^{-1}, which can be attributed to the C=O stretching vibration of ester groups originating from the nonionic surfactant (Span 20) and cholesterol present in the niosomal bilayer. In contrast, the MBSC extract-loaded niosome showed a noticeable shift of this band to a lower wavenumber, at approximately 1610 cm^{-1}, corresponding to C=C stretching

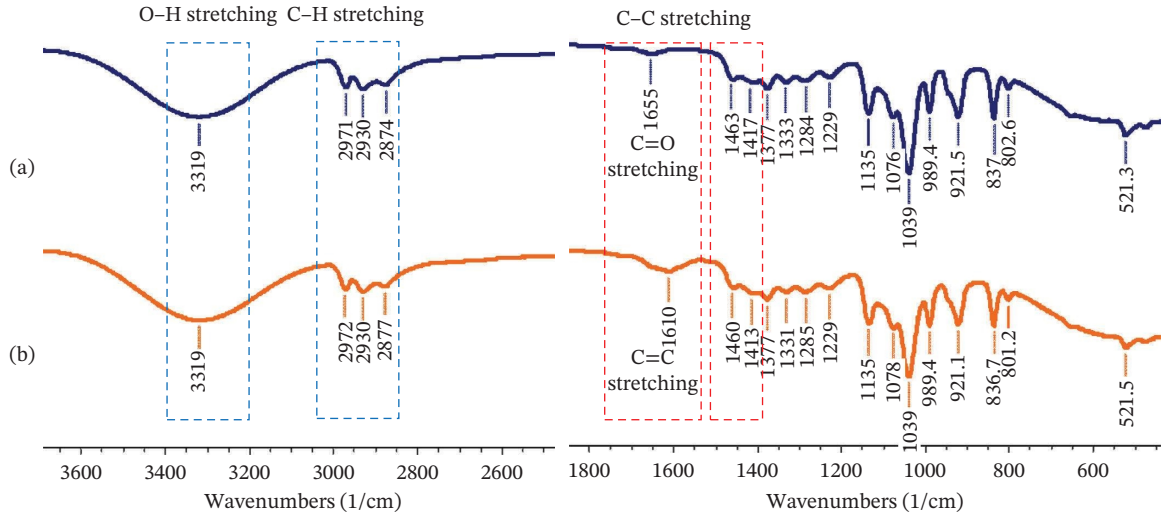


FIGURE 2 | Spectral interactions between the carbonyl functional groups. (a) Blank niosome blank (F5) and (b) MBSC-loaded niosomes (F12).

vibrations characteristic of phenolic compounds and flavonoids commonly found in MBSC extracts. The shift in the wavenumber and altered band intensity compared to the blank formulation suggest molecular interactions between the encapsulated phenolic compounds and the niosomal bilayer. This is attributed to the formation of intermolecular hydrogen bonds between the phenolic hydroxyl groups of the MBSC extract and the surfactant's carbonyl oxygen, confirming efficient molecular integration of the active component into the vesicular bilayer [34].

3.4 | The Thermal Stability of Niosome

The stability of niosome formulations was assessed under heating-cooling storage conditions. The parameters examined were zeta potential, particle size, PDI, and EE (%EE). Since TPC and TFC from MBSC may be incorporated into the niosome or interact with the bilayer membrane, these findings suggest that adding them to the niosome may improve formulation stability. However, the thermal stability test revealed significant differences ($p < 0.05$) in TPC EE and particle size (nm) for F12 before and after storage (see Table 5). In contrast, the TFC EE, PDI, and zeta potential did not differ significantly ($p > 0.05$) between F12 before and after storage. However, only the zeta potential showed a significant difference ($p > 0.05$) for F5 before and after storage.

In this study, the stability results for Formulation F12 showed a significant increase in particle size from 274.27 ± 22.10 nm to 544.83 ± 8.95 nm after storage. This increase may be attributed to aggregation or fusion of niosome particles over time, potentially caused by destabilization of the bilayer structure or reduced repulsive forces due to changes in zeta potential. As the surface charge weakens, particles may come closer together and fuse, resulting in larger particles. Additionally, the %EE of TPC in F12 decreased significantly from 77.64 ± 0.80 to 74.01 ± 0.38 ($p < 0.05$) after storage. This reduction may result from the degradation of phenolic compounds or leakage of active compounds from the niosomes due to possible membrane destabilization over time [35].

These findings highlight the importance of evaluating the long-term stability of niosome formulations, especially when intended for applications such as cosmetics or pharmaceuticals, where particle integrity and EE are critical to ensure consistent efficacy throughout product shelf life [36].

3.5 | In Vitro Release and Permeation

The MBSC extract solution and niosome formulation (F12) showed sustained release of TPC and TFC over 24 h, as indicated by the release profile in Figure 3. The MBSC extract solution exhibited rapid, high release, reaching its maximum within the

TABLE 5 | Entrapment efficiency (%), particle size, polydispersity index (PDI), and zeta potential in the stability assessment of niosome formulations.

Parameter	F5		F12	
	Before	After	Before	After
%EE				
TFC	—	—	88.17 ± 0.38	89.50 ± 1.26
TPC	—	—	77.64 ± 0.80	$74.01 \pm 0.38^{*}$
Size (nm)	162.00 ± 24.08	112.07 ± 8.15	274.27 ± 22.10	$544.83 \pm 8.95^{*}$
PDI	0.28 ± 0.05	0.25 ± 0.01	0.18 ± 0.07	0.18 ± 0.10
Zeta potential (mV)	-45.83 ± 2.20	$-63.33 \pm 0.55^{*}$	-47.70 ± 2.19	-48.50 ± 0.44

Note: Data are presented as the mean ± standard deviation (SD) from three independent experiments. Statistical comparisons were conducted using a paired *t* test, with significance defined as $^{*}p < 0.05$. This analysis was used to evaluate the stability of niosome formulations under heating–cooling storage conditions. F5 indicates the blank niosome, and F12 represents the niosome encapsulating the MBSC extract. Bold values indicate the most favorable values in terms of stability and physicochemical properties.

first 3 h and remaining relatively stable thereafter, indicating a burst-release behavior typical of free compounds in solution. In contrast, the niosome formulation (F12) displayed a sustained, controlled-release pattern, with the cumulative release of TPC and TFC at 24 h significantly lower than that of the extract solution. The release from the niosome started gradually and reached a plateau between 12 and 16 h, suggesting that the release of actives from the vesicular system slowed and stabilized, a characteristic of controlled-release systems.

At 24 h, the niosome formulation (F12) exhibited a cumulative TPC release of 29.65%, whereas the MBSC extract showed 72.74% (Figure 3(a)). Similarly, the niosome formulation (F12) exhibited a cumulative TFC release of 7.51%, while the MBSC extract showed 12.83% (Figure 3(b)).

According to the results, the niosome formulation (F12) was more successful at sustaining a regulated, extended-release profile over time, despite the extract solution delivering a higher overall release of TPC and TFC. These findings confirm that niosomes effectively delay and control the release of phenolic and flavonoid compounds, consistent with previously reported data highlighting their ability to act as sustained-release carriers. The delayed release can be attributed to the bilayer structure of niosomes, which encapsulates and protects the bioactive compounds, allowing slower diffusion across the vesicle membrane than that of the freely dissolved extract [36].

The release kinetics were evaluated by fitting the data to zero-order, first-order, Higuchi, and Korsmeyer–Peppas models. The results are summarized in Table 6, and the release kinetic plots are shown in Figures S6–S9. The release profiles of TPC and TFC from both the MBSC extract solution and the F12 niosome formulation showed the best fit to the Korsmeyer–Peppas model, indicated by the highest R^2 values. Notably, the R^2 values for TPC were 0.9553 for the MBSC extract solution and 0.9751 for F12. For TFC, the R^2 values were 0.8129 for the MBSC extract solution and 0.9586 for F12.

In addition, the release exponent (n) was determined from the slope of the linear regression of the Korsmeyer–Peppas model. The n value for TPC of F12 ($n = 0.7094$) was greater than 0.5, indicating an anomalous (non-Fickian) release mechanism involving a combination of diffusion and matrix relaxation. In contrast, the MBSC extract solution exhibited a markedly lower n value (0.1650), consistent with Fickian diffusion. The n values for TFC of the MBSC extract solution and F12 were 0.1172 and 0.2937, respectively, both indicating a diffusion-controlled (Fickian) release mechanism. The higher release exponent ($n > 0.5$) observed for TPC in F12 may be attributed to the heterogeneous nature of phenolic compounds and their interactions with the niosomal bilayer through hydrogen bonding and matrix relaxation effects [13, 37]. In contrast, the lower n values obtained for TFC suggest a diffusion-controlled-release mechanism, consistent with previous reports on flavonoid-loaded niosomes [15, 38]. The Korsmeyer–Peppas model was frequently used to describe the release kinetics of plant extract solutions and extract-loaded nanocarriers. Studies on curcumin niosomes reported non-Fickian transport [38], whereas lycopene niosomes reported a Fickian diffusion (Case I diffusional) mechanism [39], highlighting the suitability of this model for characterizing controlled release from plant-based delivery systems.

The permeation study was performed using TPC and TFC determination, as presented in Figure 4. The MBSC extract solution showed no permeation (0%) throughout the study period. The permeability parameters of Formulation F12 were evaluated and are summarized in Table 7. Formulation F12 exhibited a steady permeation across the membrane, with a flux was 1.02 ± 0.62 μg/cm^2/h. The cumulative amount of permeated compounds at 24 h (Q_{24}) was 105.10 ± 12.61 μg/cm^2, indicating effective sustained delivery. The permeability coefficient (P) was calculated to be 0.98 ± 0.59 cm^2/h, indicating effective membrane penetration. In addition, a lag time (T_{lag}) of 37.87 ± 5.32 h was observed, indicating a delayed onset of permeation before steady-state was reached. These findings collectively support the slow and prolonged transdermal delivery behavior of the F12 niosome system.

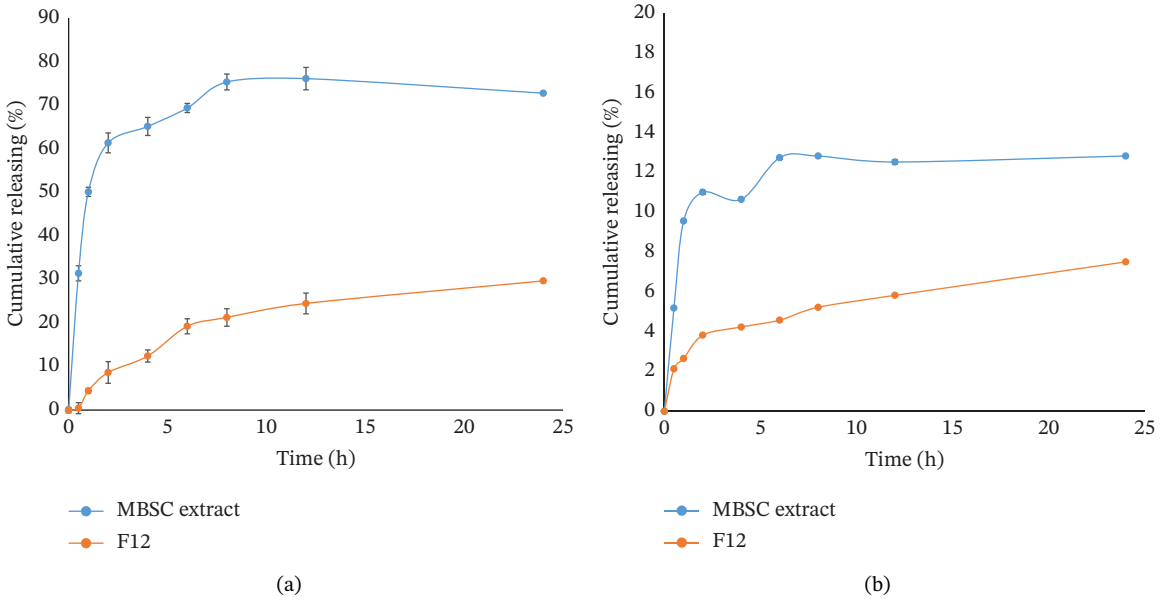


FIGURE 3 | Release profile of niosome formulation (F12) and MBSC extract: (a) total phenolic release, (b) total flavonoid release.

TABLE 6 | Kinetic release study of total phenolic (TPC) and total flavonoid content (TFC).

Content	Sample	Zero order		First order		Higuchi		Korsmeyer–Peppas	
		R^2	K_0	R^2	K_1	R^2	K_H	R^2	n
TPC	MBCS extract	0.8148	54.377	0.7714	1.7366	0.9107	43.8430	**0.9533**	0.1650
	F12	0.9176	4.9785	0.7916	0.7643	0.9744	−3.5208	**0.9751**	0.7094
TFC	MBCS extract	0.6586	10.083	0.6544	1.0036	0.7537	8.7391	**0.8129**	0.1172
	F12	0.9026	2.9699	0.8167	0.0266	0.9572	1.7743	**0.9586**	0.2937

Note: K_0 is a constant of zero-order, K_1 is a constant of first-order, K_H is a constant of the Higuchi model, n = release exponent (from the slope of the Korsmeyer–Peppas equation).

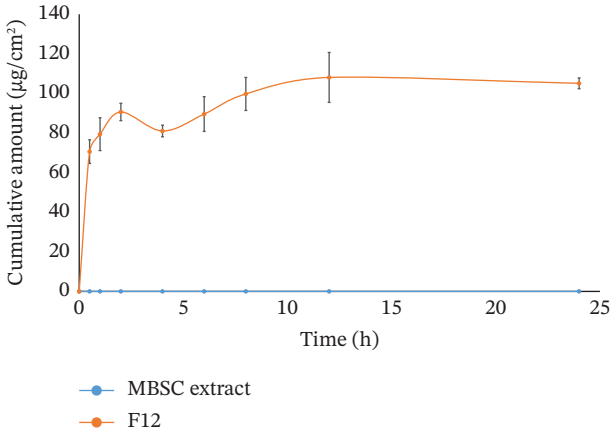


FIGURE 4 | Permeation profile of the total phenolic content.

TABLE 7 | Permeability parameters of F12.

Formulation	Flux (μg/cm²/h)	Q_{24} (μg/cm²)	P (cm²/h)	$T_{lag/h}$
F12	1.02 ± 0.62	105.10 ± 12.61	0.98 ± 0.59	37.87 ± 5.32

Note: Q_{24}: cumulative amount permeated at 24 h; P: permeability coefficient; T_{lag}: lag time.

3.6 | HPLC

HPLC analysis of the MBSC extract was performed on an Agilent 1260 system with a diode-array detector (DAD). Chromatographic separation was achieved on a Luna PFP (2) reverse-phase column (5 μm, 100 Å C18, 250 × 4.60 mm). Detection was performed at 336 nm for the quantification of vitexin and isovitexin. The injection volume was 10 μL, and the flow rate was 1.5 mL/min. The mobile phase consisted of Solvents A (1% acetic acid in water) and B (1% acetic acid in acetonitrile), applied using gradient elution as follows: 0–20 min, 95% A/5% B; 20–30 min, 80% A/20% B; 30–35 min, 78% A/22% B; 35–40 min, and 76% A/24% B, followed by re-equilibration to initial conditions. This approach enabled quantification of vitexin and isovitexin in the extract. The chromatogram of vitexin and isovitexin is presented in Figure 5, in accordance with a previously reported method [26]. The HPLC method validation confirmed high linearity for both analytes, with correlation coefficients (R^2) of 0.9997 for vitexin ($Y = 17.56x - 1.2632$) and 0.9996 for isovitexin ($Y = 15.253x - 1.5118$). The sensitivity of the method was established with LOD and LOQ values of 0.72 and 2.17 μg/mL for vitexin and 0.88 and 2.66 μg/mL for isovitexin, respectively. Precision studies demonstrated high reproducibility, with both intraday and interday relative standard deviations (%RSD) remaining below 2%. Accuracy was further confirmed by recovery rates ranging from 103.55% to 105.03% for vitexin and from 105.78% to 106.20% for isovitexin (Table 8). Quantitative analysis revealed that the crude MBSC extract contained 45.58 ± 0.46 mg/g of vitexin and 65.12 ± 0.70 mg/g of isovitexin. After encapsulation, the niosome formulations retained 29.05 ± 1.68 mg/g of vitexin and 30.68 ± 0.05 mg/g of isovitexin, confirming successful loading of these active markers into the vesicular system.

3.7 | Biological Activities of Niosome Formulation Studied

3.7.1 | UVB Protection on HaCaT Cells

Cell viability remained above 80% for all samples, indicating no cytotoxicity. Following UVB exposure (10 mJ/cm²), the nonirradiated control group showed significantly higher viability than the irradiated group (Figure 6). However, pretreatment with UVB exposure alone significantly decreased cell viability compared to the nonirradiated control group ($p > 0.05$). The MBSC extract or its niosome formulation significantly increased cell viability ($p < 0.05$) after UVB exposure, indicating protection against UVB-induced damage. The blank niosome (F1, F3, and F5) did not show any protective effects. Interestingly, the extract-loaded niosome (F12) provided the highest UVB—protection on

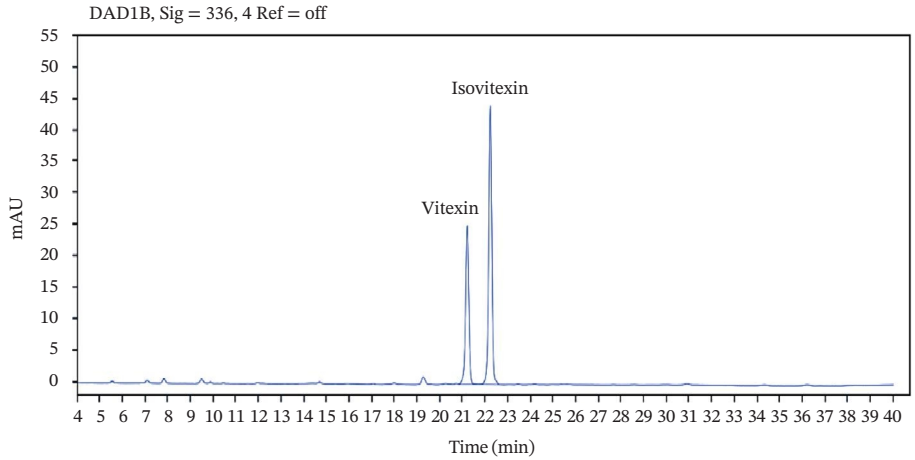


FIGURE 5 | HPLC chromatogram of standard vitexin and isovitexin with retention times of 21.4 min and 22.3 min, respectively. Analysis was performed using an Agilent 1260 HPLC system equipped with a C18 column (Luna 5 μm PFP(2), 100 Å, 250 × 4.6 mm). Separation was achieved using a gradient elution of Solvent A (1% acetic acid in water) and Solvent B (1% acetic acid in acetonitrile) at a flow rate of 1.5 mL/min as follows: 95% A/5% B (0–20 min), 80% A/20% B (20–30 min), 78% A/22% B (30–35 min), 76% A/24% B (35–40 min), followed by re-equilibration to 95% A/5% B. The injection volume was 10 μL, the column temperature was maintained at 30°C, and detection was performed using UV at 260–360 nm.

HaCaT cells. Some niosome formulations (F1, F8, F9, F10, F11, F12) performed better than the negative control, although their protective effects were lower than those of the positive control (ascorbic acid). These results suggest that, albeit slightly, encapsulating MBSC extract in niosomes can enhance its ability to protect UV-exposed skin cells from UVB-induced damage.

3.7.2 | The Collagen Production on HFF-1 Cells

Cell viability remained consistently above 80% for all samples, confirming the formulations' nontoxicity. Regarding collagen synthesis (Figure 7), pretreatment with blank niosomes (F1, F3, F5) showed negligible impact on collagen levels, confirming their noncytotoxic nature. In contrast, the MBSC extract solution modestly increased collagen compared to control, while the extract-loaded niosome (F12) significantly enhanced collagen production, surpassing both the extract alone and blank formulations and approached the level achieved with ascorbic acid positive control, all without compromising cell viability. This superior effect is attributed to the nanoscale delivery system: Niosomes facilitate deeper cellular uptake and sustained release of phytochemicals that modulate fibroblast collagen biosynthesis, as supported by previous studies showing that niosomal encapsulation increases fibroblast collagen output (e.g., gelatin-based and collagen hydrolysate-loaded niosomes) [40]. These findings suggest that MBSC-loaded niosomes not only protect bioactive compounds but also enhance their biological efficacy, offering a promising approach to the development of topical cosmetic and dermal therapeutics. Although these formulations were not as effective as ascorbic acid, they outperformed the untreated control, indicating that niosome delivery can enhance the biological effects of MBSC extract.

4 | Discussion

The present study demonstrates that encapsulating MBSC in niosomes offers significant advantages in stability, controlled release, skin permeation, and biological efficacy, highlighting its potential as an active ingredient for cosmeceutical applications. Among all formulations, F12 showed optimal physicochemical characteristics and was selected for further investigation due to its balance between high EE (%EE), nanoscale particle size, and uniform distribution. These factors are known to be critical for effective dermal delivery [41].

One of the key findings is the sustained-release profile of the F12 formulation, which showed controlled release of both TPC and TFC over 24 h, in contrast to the rapid release observed in the free extract solution. A controlled-release profile aligns with desirable characteristics for topical cosmetic products. The sustained-release property can enhance skin penetration and prolong the duration of biological action, as reported in studies of nanocarrier systems for dermal delivery [42]. Compared with conventional formulations, where rapid release may limit residence time on the skin, the profile observed in F12 suggests improved performance for applications such as antioxidant delivery, antiaging, and anti-inflammatory effects.

This controlled release can be attributed to the bilayer structure of niosomes, which slows the diffusion of active compounds into the surrounding medium [42]. The Korsmeyer–Peppas model confirmed that the release mechanism is diffusion-controlled, aligning with previous work that described niosome carriers as effective systems for prolonging the release of polyphenolic compounds [38]. The observed 24-h sustained-release profile is particularly advantageous for cosmetic applications, where a "once-daily" application regimen is preferred for consumer compliance. Sustained-release systems minimize the frequency of administration while maintaining therapeutic concentrations of bioactive compounds in the skin layers for prolonged periods. This behavior is consistent with findings for other antioxidant-loaded niosomes, such as those delivering resveratrol or curcumin, which have demonstrated that extended release (up to 24 h) significantly reduces cytotoxicity and prevents the rapid degradation of light-sensitive phenolics compared to free solutions. Furthermore, by preventing the "burst-release" effect typical of free extracts, the niosome system mitigates potential

TABLE 8 | Result of validation of HPLC for vitexin and isovitexin.

Parameter	Value (vitexin)	Value (isovitexin)
Regression equation	$Y = 17.56x - 1.2632$	$Y = 15.253x - 1.5118$
Coefficient of determination (R^2)	0.9997	0.9996
Within day (%RSD)	0.66–1.57	0.94–1.50
Between day (%RSD)	1.88–1.99	1.51–1.90
Recovery (%)	103.55–105.03	105.78–106.20
LOD (μg/mL)	0.72	0.88
LOQ (μg/mL)	2.17	2.66
Content in MBSC extract (mg/g)	45.58 ± 0.46	65.12 ± 0.70
Content in MBSC-loaded niosomes (mg/g)	29.05 ± 1.68	30.68 ± 0.05

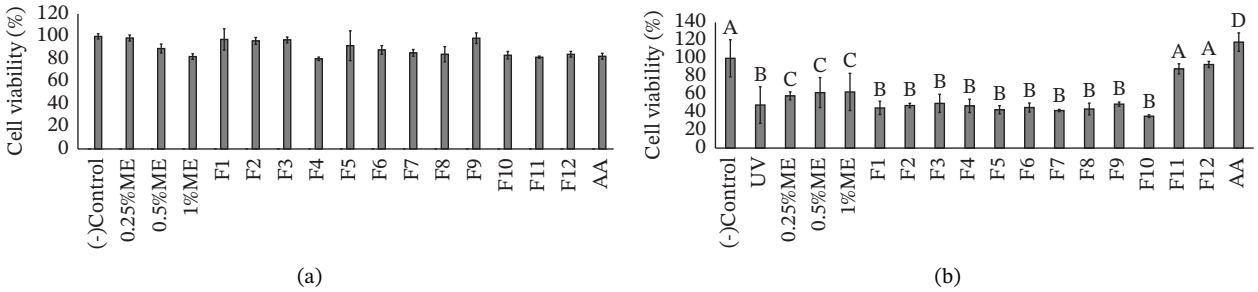


FIGURE 6 | HaCaT cell assays for UVB protection (UV): (a) without and (b) with UVB exposure following pretreatment with various concentrations of MBSC extract (ME), niosome formulations (F1-F12), and 100 μg/mL ascorbic acid (AA). Three replicate experiments (mean $\pm$ SD) were conducted, and statistical analysis was performed using Duncan's multiple-range test at $p < 0.05$. Different letters (A, B, C, D) indicate significant differences between treatment groups.

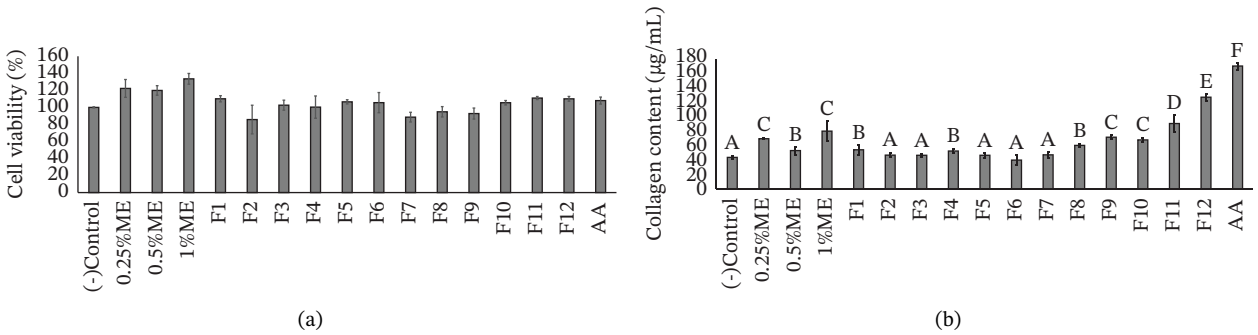


FIGURE 7 | HFF-1 cell assay for collagen stimulation: (a) Cell viability following pretreatment with various concentrations of MBSC extract (ME), niosome formulations (F1-F12), and 100 μg/mL of ascorbic acid (AA). Data were analyzed using Duncan's multiple-range test and are presented as mean $\pm$ SD from three independent experiments ($p < 0.05$). Different letters (A, B, C, D) indicate statistically significant differences between treatments. (b) Collagen content was evaluated using Sirius Red staining.

skin irritation, a critical safety parameter for leave-on cosmetic products intended for sensitive skin types [18, 43]

To confirm successful entrapment of MBSC extract within niosomes, FT-IR showed shifts in functional groups, indicating molecular interactions and incorporation into the membrane rather than surface adsorption. TEM confirmed well-defined spherical vesicles with bilayers, demonstrating proper self-assembly. Together, FT-IR and TEM verify effective encapsulation of the extract (Bautista-Solano et al. 2025). The FT-IR analysis provides strong evidence of chemical interactions between the MBSC extract and the niosome membrane components, as indicated by the noticeable shifts in some peaks and the absence of the C=O stretching vibration at 1655 cm^{-1} in MBSC-loaded niosomes compared with blank niosomes. This suggests that the extract's carbonyl groups may form hydrogen-bonding interactions with components such as Span 20 or cholesterol within the vesicular bilayer. Such interactions are critical for confirming not just passive entrapment but true molecular integration of the active compound within the delivery system. Similar findings have been reported [44], in which spectral shifts in FT-IR were used as indicators of successful encapsulation and molecular compatibility. Importantly, the

retention of other characteristic bands (e.g., O–H, C–H, C=C, C–O) indicates that the core structure of the niosome remained stable after loading, suggesting the process did not compromise the integrity of the carrier. These interactions may contribute to improved stability of the active compound, protection against environmental degradation, and potentially more controlled-release behavior. This highlights the suitability of niosome systems for delivering plant-derived actives, such as those in MBSC, which are typically sensitive to oxidation, light, and heat. Therefore, these findings support the potential use of this formulation approach to develop stable, bioavailable, and functional products for pharmaceutical or cosmeceutical applications.

Importantly, the storage stability test revealed that F12 retained most of its TFC, although a significant decrease in TPC was observed. This reduction may be due to the inherent instability of certain phenolic compounds under storage conditions or to leakage from vesicles due to slight membrane destabilization over time [45]. The increase in particle size after storage also supports this hypothesis, suggesting that vesicles may aggregate or fuse during aging.

In addition, the release profile of the active compound from Formulation F12 demonstrated sustained release for several hours, consistent with desirable characteristics for topical cosmetic products. The drug release kinetics of both the extract solution and the extract-loaded niosomes were best described by the Korsmeyer–Peppas model, as indicated by the highest R^2 value. The release exponent (n) derived from the Korsmeyer–Peppas model provided insights into the release mechanisms of the bioactive compounds. For the extract solution, n values for both the TPC ($n = 0.1650$) and TFC ($n = 0.1172$) were well below 0.43, indicating a Fickian diffusion-controlled process. In contrast, when encapsulated in niosomes, the n value for TPC increased significantly to 0.7094, suggesting an anomalous (non-Fickian) transport. This implies that the release of phenolic compounds is governed by both diffusion through the bilayer and the relaxation of the niosomal membrane. However, the n value for TFC in niosomes remained at 0.2937, signifying that flavonoids are primarily released via Fickian diffusion, possibly due to their specific localization within the niosomal structure or weaker interactions with the surfactant bilayer compared to other phenolic constituents. Sustained release can enhance skin penetration and prolong the duration of biological action, as reported in studies of nanocarrier systems for dermal delivery (Pando et al. 2013; Zazuli et al. 2025). Compared with conventional formulations, in which rapid release may limit residence time on the skin, the profile observed in F12 suggests improved performance for applications such as antioxidant delivery, antiaging, and anti-inflammatory effects.

The permeation study using a Strat-M synthetic membrane demonstrated that the niosomal formulation containing MBSC extract enhanced the transmembrane permeation of TPC compared with MBSC extract solution. Strat-M membranes are commonly used as a reproducible, ethical skin-mimicking model for the preliminary evaluation of topical formulations. Although this model does not fully replicate the complexity of biological skin tissue, the observed improvement in permeation suggests that niosomal encapsulation facilitates the transport of phenolic compounds across diffusion barriers. Further studies using excised skin or tissue-based models are warranted to confirm these findings under physiologically relevant conditions [46, 47].

This difference can be attributed to the unique properties of the niosome system. Niosomes are bilayer vesicles that can merge with the lipid layers of the stratum corneum, enhancing transdermal absorption. Additionally, their nanoscale particle size enables better penetration into the intercellular spaces. Niosomes are also effective carriers for hydrophilic compounds, which typically have poor skin permeability, by encapsulating and gradually releasing them over time. This sustained-release mechanism increases the residence time of active compounds on the skin surface, thereby improving their absorption [13]. Thus, the MBSC-loaded niosome formulation demonstrates promising potential as an efficient transdermal delivery system for phenolic compounds, especially in topical cosmetic or pharmaceutical applications.

The moderate permeability coefficient combined with a prolonged lag time indicates that drug diffusion from the F12 niosomes was governed by the structural integrity of the niosomal bilayer. The presence of cholesterol and nonionic surfactants likely enhanced membrane rigidity, thereby delaying the initial permeation. Furthermore, phenolic constituents in the extract may interact with the bilayer via hydrogen bonding, thereby reducing molecular mobility and promoting sustained release. Such characteristics are advantageous for prolonged transdermal delivery and localized therapeutic efficacy [48].

The skin permeation results further confirmed the superior performance of the niosome system. While the MBSC extract solution showed no detectable permeation of phenolics, the F12 formulation achieved a cumulative permeation of 7.92% within 24 h. This enhancement can be explained by the ability of niosomes to interact with stratum corneum lipids, fluidizing the skin barrier and promoting deeper delivery [36]. Previous research has reported similar outcomes, where niosome encapsulation significantly improved the transdermal permeation of flavonoids and polyphenols [49].

Moreover, the biological assays demonstrated that F12 not only maintained cell viability in both fibroblast (HFF-1) and keratinocyte (HaCaT) models but also significantly enhanced collagen synthesis and provided UVB protection. F12 induced collagen production at levels significantly higher than those of the MBSC solution and blank niosomes, approaching the efficacy of the positive control (ascorbic acid). This suggests that encapsulation not only preserves the activity of phenolic compounds but may also enhance their cellular uptake and bioactivity. Supporting studies have shown that niosome-encapsulated plant extracts can activate fibroblasts more effectively than free extracts [50, 51].

The biological activity of the niosome formulation observed in this study is consistent with findings for other antioxidant-loaded nanocarriers. For instance, tomato extract–loaded niosomes have been reported to provide significantly higher UVB protection in HaCaT cells than free extract, attributed to enhanced intracellular delivery of active compounds such as lycopene. [52]. Similarly, lycopene-loaded niosomes markedly increased collagen production in HFF-1 fibroblasts compared with the unencapsulated compound, validating the ability of vesicular systems to enhance the regenerative potential of phytochemicals. [53]. Furthermore, resveratrol-loaded niosomes have shown superior efficacy in stimulating collagen synthesis in fibroblasts by

improving skin penetration and drug accumulation in the dermis [54]. These comparisons confirmed that niosomal encapsulation of the MBSC extract (F12) follows a well-established pattern, in which nanocarriers enhance the stability and bioavailability of phenolic compounds, thereby maximizing their antiphotoaging and skin-rejuvenating effects.

These findings collectively suggest that MBSC extract–loaded niosomes enhance the pharmacokinetics and pharmacodynamics of plant-based actives. For MBSC extract specifically, this delivery system enables more targeted, efficient interaction with skin cells, unlocking greater cosmetic and therapeutic potential. Future work should focus on in vivo evaluations, incorporation into final topical formulations, and long-term stability assessments under different storage conditions. Compared with these materials, the performance of MBSC extract–loaded niosomes in our study demonstrates competitive UVB protection and collagen stimulation, indicating the promise of this system for topical cosmeceutical applications. Nevertheless, further direct comparative studies could provide additional insight into relative efficacy across different nanocarrier platforms.

5 | Conclusion

In conclusion, Formulation F12, a niosome delivery system containing 2% MBSC extract, formulated with Span 60 and cholesterol in a 3:2 molar ratio, demonstrated the most promising potential for topical cosmeceutical applications. F12 exhibited optimal physicochemical properties, including a particle size of 286.43 ± 15.78 nm, a PDI of 0.38 ± 0.50, and a zeta potential of -44.10 ± 1.01 mV, indicating good homogeneity and colloidal stability. The EEs were high, with $76.12 \pm 0.32\%$ for TPC and $100.68 \pm 2.39\%$ for TFC. The efficient encapsulation of the MBSC extract into niosomes via chemical interactions, specifically involving carbonyl groups, was confirmed by FT-IR spectral shifts, which also indicated improved stability and compatibility within the vesicular system. The in vitro release profile of F12 followed the Korsmeyer–Peppas kinetic model, suggesting a diffusion-controlled-release mechanism, and significantly delayed the release of active compounds compared to that of the MBSC solution. In permeation studies, F12 enhanced TPC penetration compared to the MBSC extract solution, confirming its capacity to improve dermal delivery. TEM confirmed that F12 had a spherical morphology with a well-defined bilayer structure at the nanoscale, consistent with typical niosome characteristics. Furthermore, F12 maintained stability over time, as evidenced by minimal changes in size, PDI, and zeta potential during storage. Biological evaluations showed that F12 provided UVB protection in HaCaT cells and significantly stimulated collagen production in HFF-1 fibroblasts, with greater efficacy than both the MBSC extract solution and the positive control (ascorbic acid), without causing cytotoxic effects. Altogether, these findings strongly support F12 as a stable, safe, and bioactive nanocarrier with antioxidant, antiaging, and skin-repairing properties, positioning it as a strong candidate for future development in cosmeceutical skincare products targeting oxidative damage and photoaging.

Author Contributions

Lattanamixay Souliyanon performed the experiments, performed investigation, analyzed, and interpreted the data, and reviewed and wrote the original draft. Nattawadee Kanpipit performed the experiments and performed investigation. Sakornchon Mattariganont performed the experiments and performed investigation. Suthasinee Thapphasaraphong performed conceptualized the study, proposed the methodology, provided the resources, visualized the study, curated the data, validated the study, wrote the original draft, and supervised the study and edited the manuscript.

Acknowledgments

The authors express their gratitude to Khon Kaen University's Graduate School and Pharmaceutical Sciences Scholarship for their financial assistance Thailand (Mr. Lattanamixay Souliyanon). We also acknowledge the help with the TEM imaging equipment and the access to the Zetasizer Nano ZS provided by the Research Instrument Center, Faculty of Science, Khon Kaen University. We are also grateful to Khon Kaen University's Faculty of Pharmaceutical Sciences for providing access to necessary lab space and tools, which were crucial to the accomplishment of this study.

Funding

The research on the development of MBSC (*V. radiata*) extract entrapped in niosome for topical application has received the Fundamental Fund of Khon Kaen University from National Science, Research and Innovation Fund or NSRF, Thailand (2025), and the authors also would like to thank for the Graduate student from the Faculty of Pharmaceutical Sciences of Khon Kaen University, Khon Kaen, Thailand [66-2 (2)/2566], for Mr. Lattanamixay Souliyanon.

Disclosure

All the authors have approved the final article.

Conflicts of Interest

The authors declare no conflicts of interest.

Data Availability Statement

The data used to support the findings of this study are included within the article.

References

1. M. E. Manful, L. Ahmed, and C. Barry-Ryan, "Cosmetic Formulations from Natural Sources: Safety Considerations and Legislative Frameworks in the European Union," *Cosmetics* 11, no. 3 (2024): 72, https://doi.org/10.3390/cosmetics11030072.

2. L. E. Bejenaru, A. Radu, A.-E. Segneanu, et al., "Innovative Strategies for Upcycling Agricultural Residues and Their Various Pharmaceutical Applications," *Plants* 13, no. 15 (2024): 2133, https://doi.org/10.3390/plants13152133.

3. M. Tarahi, "The Potential Application of Mung Bean (Vigna radiata L.) Protein in Plant-Based Food Analogs: A Review," *Legume Science* 6, no. 4 (2024): e70011, https://doi.org/10.1002/leg3.70011.

4. Ai-P. Li, Z.-Y. Li, J.-P. Jia, and X.-M. Qin, "Chemical Comparison of Coat and Kernel of Mung Bean by Nuclear Magnetic Resonance-Based Metabolic Fingerprinting Approach," *Spectroscopy Letters* 49, no. 3 (2016): 217–224, https://doi.org/10.1080/00387010.2015.1133648.

5. J. Luo, W. Cai, T. Wu, and B. Xu, "Phytochemical Distribution in Hull and Cotyledon of Adzuki Bean (*Vigna angularis* L.) and Mung Bean (*Vigna radiate* L.), and Their Contribution to Antioxidant, Anti-Inflammatory and Anti-Diabetic Activities," *Food Chemistry* 201 (2016): 350–360, https://doi.org/10.1016/j.foodchem.2016.01.101.

6. P. K. Dahiya, A. R. Linnemann, M. A. J. S. Van Boekel, N. Khetarpaul, R. B. Grewal, and M. J. R. Nout, "Mung Bean: Technological and Nutritional Potential," *Critical Reviews in Food Science and Nutrition* 55, no. 5 (2015): 670–688, https://doi.org/10.1080/10408398.2012.671202.

7. D. Hou, L. Yousaf, Y. Xue, et al., "Mung Bean (*Vigna radiata* L.): Bioactive Polyphenols, Polysaccharides, Peptides, and Health Benefits," *Nutrients* 11, no. 6 (2019): 1238, https://doi.org/10.3390/nu11061238.

8. Y. M. Jeong, Ji H. Ha, G. Y. Noh, and S. N. Park, "Inhibitory Effects of Mung Bean (Vigna radiata L.) Seed and Sprout Extracts on Melanogenesis," *Food Science and Biotechnology* 25, no. 2 (2016): 567–573, https://doi.org/10.1007/s10068-016-0079-6.

9. N. Mehta, P. Rao, and R. Saini, "A Review on Metabolites and Pharmaceutical Potential of Food Legume Crop Mung Bean (Vigna radiata L. Wilczek)," *BioTechnologia* 102, no. 4 (2021): 425–435, https://doi.org/10.5114/bta.2021.111107.

10. W.-M. Chai, C. Ou-Yang, Q. Huang, et al., "Antityrosinase and Antioxidant Properties of Mung Bean Seed Proanthocyanidins: Novel Insights into the Inhibitory Mechanism," *Food Chemistry* 260 (2018): 27–36, https://doi.org/10.1016/j.foodchem.2018.04.001.

11. R. L. McMullen and G. Dell'Acqua, "History of Natural Ingredients in Cosmetics," *Cosmetics* 10, no. 3 (2023): 71, https://doi.org/10.3390/cosmetics10030071.

12. S. Gupta, R. Bansal, S. Gupta, N. Jindal, and A. Jindal, "Nanocarriers and Nanoparticles for Skin Care and Dermatological Treatments," *Indian Dermatology Online Journal* 4, no. 4 (2013): 267, https://doi.org/10.4103/2229-5178.120635.

13. S. Moghassemi and A. Hadjizadeh, "Nano-Niosomes as Nanoscale Drug Delivery Systems: An Illustrated Review," *Journal of Controlled Release* 185 (2014): 22–36, https://doi.org/10.1016/j.jconrel.2014.04.015.

14. S. Jacob, F. S. Kather, S. H. S. Boddu, R. Rao, and A. B. Nair, "Vesicular Carriers for Phytochemical Delivery: A Comprehensive Review of Techniques and Applications," *Pharmaceutics* 17, no. 4 (2025): 464, https://doi.org/10.3390/pharmaceutics17040464.

15. A. Priprem, K. Janpim, S. Nualkaew, and P. Mahakunakorn, "Topical Niosome Gel of *Zingiber Cassumunar* Roxb. Extract for Anti-Inflammatory Activity Enhanced Skin Permeation and Stability of Compound D," *AAPS PharmSciTech* 17, no. 3 (2016): 631–639, https://doi.org/10.1208/s12249-015-0376-Z.

16. N. Ibrahim, H. Abbas, N. S. El-Sayed, and H. A. Gad, "Rosmarinus Officinalis L. Hexane Extract: Phytochemical Analysis, Nanoencapsulation, and in Silico, in Vitro, and in Vivo Anti-Photoaging Potential Evaluation," *Scientific Reports* 12, no. 1 (2022): 13102, https://doi.org/10.1038/s41598-022-16592-7.

17. A. A. Abd-Elghany and E. A. Mohamad, "Chitosan-Coated Niosomes Loaded with Ellagic Acid Present Antiaging Activity in a Skin Cell Line," *ACS Omega* 8, no. 19 (2023): 16620–16629, https://doi.org/10.1021/acsomega.2c07254.

18. S. M. Mawazi, Jo A. Tong, and R. T. Widodo, "Application of Niosomes in Cosmetics: A Systematic Review," *Cosmetics* 9, no. 6 (2022): 127, https://doi.org/10.3390/cosmetics9060127.

19. H. M. Aung, N. Kanpipit, and S. Thapphasaraphong, "Effects of Thanaka (Hesperethusa Crenulata) Stem Bark Extract on Collagen Activation and Anti-Melanogenesis for Cosmetic Applications," *Tropical Journal of Natural Product Research (TJNPR)* 8, no. 1 (2024): 5852–5860.

20. D. D. Sylvie, P. Constant Anatole, B. P. Cabral, and P. B. Veronique, "Comparison of in Vitro Antioxidant Properties of Extracts from Three Plants Used for Medical Purpose in Cameroon: Acalypha racemosa, Garcinia lucida and Hymenocardia lyrata," *Asian Pacific Journal of Tropical Biomedicine* 4 (2014): S625–S632, https://doi.org/10.12980/APJTB.4.201414B168.

21. I. Biskup, I. Golonka, A. Gamian, and Z. Sroka, "Antioxidant Activity of Selected Phenols Estimated by ABTS and FRAP Methods," *Postępy Higieny I Medycyny Doświadczalnej* 67 (2013): 958–963, https://doi.org/10.5604/17322693.1066062.

22. H. Gorjian, Z. R. Amiri, J. M. Milani, and N. G. Khaligh, "Preparation and Characterization of the Encapsulated Myrtle Extract Nanoliposome and Nanoniosome Without Using Cholesterol and Toxic Organic Solvents: A Comparative Study," *Food Chemistry* 342 (2021): 128342, https://doi.org/10.1016/j.foodchem.2020.128342.

23. P. Wichayapreechar, S. Anuchapreeda, R. Phongpradist, W. Rungseevijitprapa, and C. Ampasavate, "Dermal Targeting of *Centella asiatica* Extract Using Hyaluronic Acid Surface Modified Niosomes," *Journal of Liposome Research* 30, no. 2 (2020): 197–207, https://doi.org/10.1080/08982104.2019.1614952.

24. M. Bragagni, N. Mennini, C. Ghelardini, and P. Mura, "Development and Characterization of Niosomal Formulations of Doxorubicin Aimed at Brain Targeting," *Journal of Pharmacy & Pharmaceutical Sciences* 15, no. 1 (2012): 184, https://doi.org/10.18433/J3230M.

25. N. Kanpipit, N. Nualkaew, W. Kiatponglarp, A. Priprem, and S. Thapphasaraphong, "Development of a Sericin Hydrogel to Deliver Anthocyanins from Purple Waxy Corn Cob (*Zea Mays* L.) Extract and in Vitro Evaluation of Anti-Inflammatory Effects," *Pharmaceutics* 14, no. 3 (2022): 577, https://doi.org/10.3390/pharmaceutics14030577.

26. H. Salhab and J. Barker, "Development and Validation of an HPLC-UV Method for the Quantification of 4′-Hydroxydiclofenac Using Salicylic Acid: Future Applications for Measurement of in Vitro Drug–Drug Interaction in Rat Liver Microsomes," *Molecules* 27, no. 11 (2022): 3587, https://doi.org/10.3390/molecules27113587.

27. D. Cao, L. He, J. Yi, et al., "Antioxidant Properties of the Mung Bean Flavonoids on Alleviating Heat Stress," *PLoS One* ed. V. Saks, 6, no. 6 (2011): e21071, https://doi.org/10.1371/journal.pone.0021071.

28. W. Pabuprapap, W. Nakyai, W. Chaichompoo, et al., "Curcuma aromatica and Curcuma comosa Extracts and Isolated Constituents Provide Protection Against UVB-Induced Damage and Attenuate Matrix Metalloproteinase-1 Expression in Hacat Cells," *Cosmetics* 9, no. 1 (2022): 23, https://doi.org/10.3390/cosmetics9010023.

29. Y. Zhou, J. Zheng, R.-Y. Gan, Z. Tong, D.-P. Xu, and H.-B. Li, "Optimization of Ultrasound-Assisted Extraction of Antioxidants from the Mung Bean Coat," *Molecules* 22, no. 4 (2017): 638, https://doi.org/10.3390/molecules22040638.

30. B. Supasatyankul, M. Saisriyoot, U. Klinkesorn, K. Rattanaporn, and S. Sae-Tan, "Extraction of Phenolic and Flavonoid Compounds from Mung Bean (Vigna radiata L.) Seed Coat by Pressurized Liquid Extraction," *Molecules* 27, no. 7 (2022): 2085, https://doi.org/10.3390/molecules27072085.

31. M. Danaei, M. Dehghankhold, S. Ataei, et al., "Impact of Particle Size and Polydispersity Index on the Clinical Applications of Lipidic Nanocarrier Systems," *Pharmaceutics* 10, no. 2 (2018): 57, https://doi.org/10.3390/pharmaceutics10020057.

32. V. B. Junyaprasert, V. Teeranachaideekul, and T. Supaperm, "Effect of Charged and Non-Ionic Membrane Additives on Physicochemical Properties and Stability of Niosomes," *AAPS PharmSciTech* 9, no. 3 (2008): 851, https://doi.org/10.1208/s12249-008-9121-1.

33. S. Asthana, Gyati, P. K. Sharma, and A. Asthana, "In Vitro and in Vivo Evaluation of Niosomal Formulation for Controlled Delivery of Clarithromycin," *Scientific* 2016, no. 1 (2016): 6492953, https://doi.org/10.1155/2016/6492953.

34. A. Ababei-Bobu, B.-Ş. Profire, A.-T. Iacob, O.-M. Chirliu, F. G. Lupaşcu, and L. Profire, "Niosomes as Vesicular Carriers: From Formulation Strategies to Stimuli-Responsive Innovative Modulations for Targeted Drug Delivery," *Pharmaceutics* 17, no. 11 (2025): 1473, https://doi.org/10.3390/pharmaceutics17111473.

35. R. Vaiswade, S. Chandrakar, A. Roy, and P. Prasad, "Stability Aspects of Niosome" (2020).

36. S. Pandey, S. Kaur, P. Verma, A. P. Singh, and A. P. Singh, "Comprehensive Review of Niosomes as Advanced Drug Delivery System," *International Journal of Pharmaceutical Research and Development* 7, no. 1 (2025): 297–304, https://doi.org/10.33545/26646862.2025.v7.i1d.123.

37. R. W. Korsmeyer, R. Gurny, E. Doelker, P. Buri, and N. A. Peppas, "Mechanisms of Solute Release from Porous Hydrophilic Polymers,"

International Journal of Pharmaceutics 15, no. 1 (1983): 1–35, https://doi.org/10.1016/0378-5173(83)90064-9.

38. T. M. Shehata, M. M. Ibrahim, and H. S. Elsewedy, "Curcumin Niosomes Prepared from Proniosomal Gels: In Vitro Skin Permeability, Kinetic and in Vivo Studies," *Polymers* 13, no. 5 (2021): 791, https://doi.org/10.3390/polym13050791.

39. N. Kanpipit, S. Mattariganont, P. Janphuang, et al., "Comparative Study of Lycopene-Loaded Niosomes Prepared by Microfluidic and Thin-Film Hydration Techniques for UVB Protection and Anti-Hyperpigmentation Activity," *International Journal of Molecular Sciences* 25, no. 21 (2024): 21, https://doi.org/10.3390/ijms252111717.

40. C. Szász, D. Pap, B. Szebeni, et al., "Optimization of Sirius Red-Based Microplate Assay to Investigate Collagen Production in Vitro," *International Journal of Molecular Sciences* 24, no. 24 (2023): 17435, https://doi.org/10.3390/ijms242417435.

41. E. Mazzotta, C. Orlando, and R. Muzzalupo, "New Nanomaterials with Intrinsic Antioxidant Activity by Surface Functionalization of Niosomes with Natural Phenolic Acids," *Pharmaceutics* 13, no. 6 (2021): 766, https://doi.org/10.3390/pharmaceutics13060766.

42. A. Azeem, Md. Khalid Anwer, and S. Talegaonkar, "Niosomes in Sustained and Targeted Drug Delivery: Some Recent Advances," *Journal of Drug Targeting* 17, no. 9 (2009): 671–689, https://doi.org/10.3109/10611860903079454.

43. P. Ganesan and K. C. Dong, "Current Application of Phytocompound-Based Nanocosmeceuticals for Beauty and Skin Therapy," *International Journal of Nanomedicine* 1987 (2016): https://doi.org/10.2147/IJN.S104701.

44. M. Khan, M. A. Madni, S. Ahmad, A. Khan, M. Rehman, and M. Mahmood, "ATR-FTIR Based Pre and Post Formulation Compatibility Studies for the Design of Niosomal Drug Delivery System Containing Nonionic Amphiphiles and Chondroprotective Drug," *Journal of the Chemical Society of Pakistan* 37 (2015).

45. A. C. Santos, F. Morais, A. Simões, et al., "Nanotechnology for the Development of New Cosmetic Formulations," *Expert Opinion on Drug Delivery* 16, no. 4 (2019): 313–330, https://doi.org/10.1080/17425247.2019.1585426.

46. H. Kichou, F. Bonnier, Y. Dancik, et al., "Strat-M® Positioning for Skin Permeation Studies: A Comparative Study Including Episkin® RHE, and Human Skin," *International Journal of Pharmaceutics* 647, no. November (2023): 123488, https://doi.org/10.1016/j.ijpharm.2023.123488.

47. T. Uchida, W. R. Kadhum, S. Kanai, H. Todo, T. Oshizaka, and K. Sugibayashi, "Prediction of Skin Permeation by Chemical Compounds Using the Artificial Membrane, Strat-M™," *European Journal of Pharmaceutical Sciences* 67 (2015): 113–118, https://doi.org/10.1016/j.ejps.2014.11.002.

48. R. Muzzalupo and L. Tavano, "Niosomal Drug Delivery for Transdermal Targeting: Recent Advances," *Research and Reports in Transdermal Drug Delivery* 4, no. July (2015): 23–33, https://doi.org/10.2147/RRTD.S64773.

49. S. Al, M. A. Ahmed, I. Poudel, et al., "Niosomal Formulation of Hydroxytyrosol, a Polyphenolic Antioxidant, for Enhancing Transdermal Delivery Across Human Cadaver Skin," *Pharmaceutical Development and Technology* 27, no. 2 (2022): 155–163, https://doi.org/10.1080/10837450.2022.2025540.

50. P. Jantrawut, T. Akihisa, W. Manosroi, and J. Manosroi, "In Vitro and in Vivo Skin Anti-Aging Evaluation of Gel Containing Niosomes Loaded with a Semi-Purified Fraction Containing Gallic Acid from Terminalia chebula Galls," *Pharmaceutical Biology* 49, no. 11 (2011): 1190–1203, https://doi.org/10.3109/13880209.2011.576347.

51. M. Lens, "Niosomes as Vesicular Nanocarriers in Cosmetics: Characterisation, Development and Efficacy," *Pharmaceutics* 17, no. 3 (2025): 287, https://doi.org/10.3390/pharmaceutics17030287.

52. N. Kanpipit, S. Mattariganont, L. Temprom, et al., "Response Surface Methodology-Optimized Niosomes Encapsulating Whole Tomato Extract: Release Profile and Mechanistic Insights for UVB Protection and Anti-Melanogenesis Applications," *Open* 27 (2026): 100267, https://doi.org/10.1016/j.onano.2025.100267.

53. N. Kanpipit, S. Mattariganont, L. Temprom, et al., "Ball-Milling-Assisted Extraction and Niosomal Delivery of Lycopene from Gac Fruit for Enhanced Physicochemical Properties, Drug Delivery, Anti-Inflammatory, and Collagen Stimulation," *Journal of Dispersion Science and Technology* 0, no. 0 (2025): 1–14, https://doi.org/10.1080/01932691.2025.2566256.

54. W. T. Chen and J. L. Wen, "Advanced Hyaluronic Acid-Modified Niosomes for Percutaneous Delivery of Resveratrol in the Treatment of Aged Skin," *International Journal of Biological Macromolecules* 325 (2025): 147250, https://doi.org/10.1016/j.ijbiomac.2025.147250.

Supporting Information

Additional supporting information can be found online in the Supporting Information section. *(Supporting Information)*

Supporting Information, including Figure S1. Extraction of the MBSC with 40% ethanol by the Soxhlet method, Figure S2. The formulations of niosome (F1–F12), Figure S3. FT-IR spectra of niosomes prepared by sonication: (A) MBSC extract, (B) blank niosome (F5), and (C) MBSC-loaded niosomes (F12). Figure S4. FT-IR spectra of (A) Span20, (B) cholesterol, and(C) PG, Figure S5. Size distribution and PDI (A, B, C) and zeta potential (D, E, F) of niosome Formulation F12, Figure S6. Release kinetics graphs of TPC from MBCS extract (A) zero-order, (B) first order, (C) Higuchi, and (D) Korsmeyer–Peppas, Figure S7. Release kinetics graphs of TPC from F12: (A) zero-order, (B) first order, (C) Higuchi, and (D) Korsmeyer–Peppas, Figure S8. Release kinetics graphs of TFC from the MBCS extract: (A) zero order, (B) first order, (C) Higuchi, and (D) Korsmeyer–Peppa, Figure S9. Release kinetics graphs of TFC from F12: (A) Zero order, (B) first order, (C) Higuchi, and (D) Korsmeyer–Peppas, Table S1. The wave number of the MBSC extract, niosome blank (F5), and MBSC-loaded niosomes (F12), Table S2. The wave number of Span20, cholesterol, and propylene glycol, Table S3. Average size distribution, PDI, and zeta potential of niosome Formulation F12 ($n = 3$).